Development of a functional genetic tool for Anopheles gambiae oenocyte characterisation: application to cuticular hydrocarbon synthesis

Amy Lynd[*], Vasileia Balabanidou[†], Rudi Grosman[+], James Maas[*], Lu-Yun Lian[+], John Vontas[†‡] and Gareth J. Lycett[*]

* Vector Biology Dept, Liverpool School of Tropical Medicine, Liverpool, L3 5QA, UK

† Institute of Molecular Biology and Biotechnology, Foundation for Research and Technology-Hellas, Heraklion 70013, Greece

+ Institute of Integrative Biology, University of Liverpool, Liverpool, UK

‡ Department of Crop Science, Agricultural University of Athens, 11855 Athens, Greece

Short title: mosquito oenocyte function

Keywords: cytochrome P450, gene knockdown, malaria, enhancer, Gal4 driver

Corresponding Author
Dr. Gareth Lycett
Vector Biology Dept.
Liverpool School of Tropical Medicine
Pembroke Place
Liverpool
L3 5QA
UK

Tel 44 151 7053137
Email Gareth.Lycett@lstmed.ac.uk

Abstract

Oenocytes are an insect cell type having diverse physiological functions ranging from cuticular hydrocarbon (CHC) production to insecticide detoxification that may impact their capacity to transmit pathogens. To develop functional genetic tools to study *Anopheles gambiae* oenocytes, we have trapped an oenocyte enhancer to create a transgenic mosquito Gal4 driver line that mediates tissue-specific expression. After crossing with UAS-reporter lines, *An. gambiae* oenocytes are fluorescently tagged through all life stages and demonstrate clearly the two characteristic oenocyte cell-types arising during development. The driver was then used to characterise the function of two oenocyte expressed *An. gambiae cyp4g* genes through tissue-specific expression of UAS-RNAi constructs. Silencing of *cyp4g16* or *cyp4g17* caused lethality in pupae of differing timing and penetrance. Surviving *cyp4g16* knockdown adults showed increased sensitivity to desiccation. Total cuticular hydrocarbon levels were reduced by approximately 80% or 50% in both single gene knockdowns when assayed in young pupa or surviving adults respectively, indicating both genes are required for complete CHC production in *An. gambiae* and demonstrate synergistic activity in young pupae. Comparative CHC profiles were very similar for the two knockdowns, indicating overlapping substrate specificities of the two enzymes. Differences were observed for example with reduced abundance of shorter chain CHCs in CYP4G16 knockdowns, and reduction in longer, branched chained CHCs in CYP4G17 knockdown adults. This is the first time that two *cyp4g*s have both been shown to be required for complete CHC production in an insect. Moreover, the generation of tagged cells and identification of an enhancer region can expediate oenocyte specific transcriptomics. The novel

51 driver line can also be used to explore oenocyte roles in pheromone production,
52 mating behaviour and longevity in the malaria mosquito.

53

54

55 **Introduction**

56 Oenocytes are insect secretory cells that in diptera such as Drosophila exist as
57 morphologically distinct derivatives in larvae and adults with separate developmental
58 origins (Gould et al. 2001). In the fruitfly, larval oenocytes originate from embryonic
59 ectodermal cells, whereas adult oenocytes are thought to derive from pupal
60 histoblasts (Makki et al. 2014). These liver-like cells that have diverse physiological
61 functions encompassing regulation of respiration, tissue histolysis, detoxification,
62 hormone production, dietary related longevity and cuticle synthesis (Makki et al.
63 2014; Stefana et al. 2017). Perhaps best studied to date are those roles linked to
64 lipid metabolism. Fruitfly oenocytes express an abundance of lipid synthesis
65 enzymes, including those in the pathways leading to the production of very long
66 chain (VLC) lipids and cuticular hydrocarbons (CHC) (Gutierrez et al. 2007). These
67 are transported to the tracheal system and outer insect integument to provide a
68 hydrophobic waxy layer to maintain water balance (Parvy et al. 2012). This key
69 adaptive trait provides insects with the ability to limit dehydration, yet repel water to
70 prevent flooding, in order to occupy different niches. The precise control of CHC
71 composition to maintain water balance is compounded in insects with aquatic
72 immature stages, including mosquitoes, which must switch rapidly during pupal
73 development from submersion in water to an environment with variable humidity.

74 Our interest in developing genetic tools to study mosquito oenocytes stems from an
75 initial observation that the sole reductive binding partner, cytochrome p450
76 reductase (CPR), of the largest family of multifunctional oxidative enzymes, the
77 cytochromes P450 (CYPs), was massively expressed in these cells, in both *An.*
78 *gambiae* and Drosophila (Lycett et al. 2006). Later studies in Drosophila linked
79 expression of CPR and a single CYP4G partner, CYP4G1 in oenocytes with the final
80 decarbonylation step in the cuticular hydrocarbon synthetic pathway that converts
81 VLC aldehydes to alkanes and alkenes (Qiu et al. 2012a). Similar activity has
82 recently been detected in the single *cyp4g* gene encoded in the honey bee genome
83 (Calla et al. 2018). In contrast two *cyp4g* genes are annotated in the Anopheles
84 genome, *cyp4g16* and *cyp4g17*, and we have previously shown that both gene
85 products are highly expressed in adult and pupal oenocytes (Kefi et al. 2019; Ingham
86 et al. 2014; Balabanidou et al. 2016), yet only CYP4G16 had decarbonylase activity
87 *in vitro*. In other species with two annotated members of the *cyp4*g family, both
88 recombinant enzymes possess decarbonylase activity (MacLean et al. 2018), and
89 when the Anopheles genes were expressed in Drosophila in a *cyp4g1* silenced
90 background either enzyme or in combination rescued the lethal phenotype (Kefi et al.
91 2019). The observed inactivity of the recombinant *An. gambiae* CYP4G17 is thus
92 most likely due to incompatibility with the low molecular weight substrate aldehyde
93 that was tested *in vitro* (Balabanidou et al. 2016).

94 To expand the *in vivo* analysis of oenocyte function in mosquitoes, we have
95 developed a Gal4 driver line to modify gene expression specifically in *An. gambiae*
96 oenocytes, and have initially targeted the *cyp4g* genes. Our earlier research
97 identified a number of Gal4 activators and UAS modules suitable for expression in
98 *An. gambiae* (Lynd and Lycett 2012, 2011). Moreover, in creating a series of docking

99 lines for recombinase mediated cassette exchange (Pondeville et al. 2014), we
100 serendipitously created a transgenic line in which ectopic expression of the normally
101 eye specific fluorescent marker gene was observed in larval, pupal and adult
102 oenocytes. By cassette exchange of this marker with promoterless Gal4 activators,
103 we tested whether the putative oenocyte enhancer could be trapped to drive Gal4
104 expression. Following successful enhancer trapping, we then examined the *in vivo*
105 role of the two *An. gambiae cyp4g* genes by stable RNAi using UAS:hairpin DNA
106 constructs regulated by the oenocyte Gal4 driver.

107

108 **Materials and Methods**

109 ***Plasmid construction***

110 **pBac-CFP**

111 The docking lines were created via transformation of *Anopheles gambiae* embryos
112 using a *piggyBac* vector containing the leucine-rich repeat protein immunity gene,
113 LRIM1(Povelones et al. 2009), under the control of the *vitellogenin promoter*, *Vg*,
114 with an eCFP 3xP3 eye marker gene (Horn et al. 2000), flanked by inverted *attP*
115 sequences. The *vitellogenin* promoter, *Vg*, (AGAP013109) was removed from
116 pBac[3xP3DsRed-AgVgT2-GFP] (Chen et al. 2008) with AscI and subcloned into
117 pSLfa1180fa (Horn and Wimmer 2000) to give pslVg-GFP-BGH, which was
118 subsequently digested with EcoRI and BamHI and the *Vg* promoter cloned into
119 pSLfa1180fa.
120 BGH was amplified by PCR from pslVg-GFP-BGH by PCR with BamHI and NotI
121 tagged primers (BGH-F, BGH-R) and subcloned into pJET1.2 (Thermo Scientific).
122 *attP* was amplified from pBCPB+ (Groth et al. 2000) with XhoI and NotI tagged

123 primers (attP-F, attP-R) and subcloned into pJET1.2. pslVg was digested with
124 BamHI and XhoI, and the BGH and *attP* fragments, removed from pJET1.2 by
125 BamHI /NotI and XhoI/NotI digests respectively, were cloned into pslVg
126 simultaneously. LRIM1 (AGAP006348) with Strep and His epitope tags was
127 amplified by PCR from pIEx10-LRIM1 (Povelones et al. 2009) with BamHI tagged
128 primers (LRIM1-F, LRIM1-R) and subcloned into pJET1.2 (Thermo Scientific) before
129 cloning into pslVg-BGH-attP. *attP* was released from pBac[3xP3-eCFPaf]-attP
130 (Nimmo et al. 2006) by digestion with PstI, and *attP* reinserted in the opposite
131 orientation by PCR amplification of *attP* from pBCPB+ with PstI tagged primers
132 (attPPSTI-F, attPPSTI-R) to make pBac[3xP3-eCFPaf]-attPii. pslVg-LRIM1-BGH-
133 attP was digested with AscI and cloned into pBac[3xP3-eCFPaf]-attPii to give pBac-
134 CFP (Fig S1). All primers used are shown in Table S1.

135 **pSL-attB-Hsp-Gal4(3xP3-dsRed)**

136 RCME was carried out via PhiC31 recombination in the *attP* docking lines using a
137 plasmid containing a minimal promoter upstream of a Gal4 coding region, and a
138 dsRed 3XP3 marker (Horn et al. 2002) and flanked by inverted attB sites to allow
139 cassette replacement via a double recombination event.
140 The minimal heat shock promoter Hsp70 was amplified by PCR from pUAST (Brand
141 and Perrimon 1993) with NotI and EcoRI tagged primers (HSP-F, HSP-R), and
142 subcloned into psl-LRIM-Gal4Δ and psl-LRIM-Gal4FF (Lynd and Lycett 2011) in
143 place of the LRIM promoter. The 5' attB site was amplified from pB*attB*[3×P3-
144 dsRed2nls-SV40]/*ox*66 using AflII and SpeI tagged (attB5-F, attB-R) primers and
145 ligated into psl-Hsp-Gal4Δ and psl-Hsp-Gal4FF. A synthetic multiple cloning site was
146 inserted into the 3' unique BamHI site to provide EcoRI, SphI, NheI, NsiI and BglII
147 sites. The 3' attB site was subcloned into both Gal4 plasmids after PCR

148 amplification from pB*attB*[3×P3-dsRed2nls-SV40]/*ox*66 (Nimmo et al. 2006) using
149 BglII and NsiI tagged primers (attB3-F, attB3-R). The 3xP3 promoter, dsRed gene
150 and SV40 region were amplified from pBac[3×P3-dsRed] (Horn et al. 2002) using
151 NheI and NsiI tagged primers (Red-F, Red-R) and subcloned downstream of the
152 Hsp-gal4 cassette. Plasmids psl-attB-Hsp-Gal4[3xP3dsRed] and psl-attB-Hsp-
153 Gal4GFY[3xP3DsRed] were constructed by subcloning Gal4 and Gal4GFY
154 fragments from pLRIM-Gal4 and pLRIM-Gal4-GFY respectively (Lynd and Lycett
155 2011), into Psl-attB-Hsp-Gal4Δ[3xP3dsRed] in place of Gal4Δ using enzymes EcoRV
156 and PspXI. All regions amplified by PCR were sequenced and all plasmids verified
157 by diagnostic restriction digest (primers shown in Table S1).

158 **pSL-attB-UAS-cyp16RNAi and pSL-attB-UAS-cyp17RNAi**

159 To create a suitable UAS vector for expressing hairpin RNAi cassettes, the luciferase
160 gene was removed from pUAS14-LUC (Lynd and Lycett 2011) by digestion with NcoI
161 and XbaI and the plasmid was re-ligated using an oligo linker. The gypsy insulator
162 sequence from pH-Stinger (Drosophila Genomic Resource Centre) (Barolo et al.
163 2000) was amplified by PCR with HindIII and SphI tagged primers (gyp1F, gyp1R)
164 and inserted 5′ to the UAS. A second gypsy insulator sequence was inserted 3’ via
165 PCR amplification using BamHI tagged primers (gyp2F, gyp2R). A multiple cloning
166 site was then inserted into resultant plasmid by linker insertion (RINcoF, RINcoR)
167 following EcoRI and NcoI digestion. Fusion PCR was carried out to create an *eYFP*
168 marker under the control of the 3xP3 promoter with an SV40 terminator from
169 plasmids eYFP-mem (Clontech), pBac[3×P3-dsRed]CP-Gal4-GFY-SV40 (Lynd and
170 Lycett 2012) and pSL-attB-Hsp-Gal4[3xP3-dsRed] respectively. This cassette was
171 cloned into the above UAS-gypsy intermediate plasmid with NsiI to give pSL-UAS14-
172 gyp[3×P3-eYFP]. pSL-attB-Hsp-Gal4[3xP3-dsRed] was digested with NsiI and NotI

173 and religated with an oligo linker (Link2F, Link2R) to give pSL-attB. pSL-UAS14-
174 gyp[3×P3-eYFP] was digested with NotI and SpeI and the entire cassette ligated into
175 pSL-attB to give pSL-attB-UAS14-gyp[3×P3-eYFP] (primers shown in Table S1).
176
177 To create the *cyp4g16* knockdown construct, genomic DNA (gDNA) was extracted
178 from adult *Anopheles gambiae* females (G3 strain) using the method described in
179 Livak (1984). A hairpin RNAi construct was then generated by direct amplification via
180 asymmetric PCR of gDNA (Xiao et al. 2006) using exon 2 of *cyp4g16*
181 (AGAP001076) to form the double stranded stem (198bp) and intron 2 to form the
182 loop (579bp). PCR was carried out in a 25 µl reaction volume containing a final
183 concentration of 1× HF buffer (ThermoScientific), 2.5 mM dNTPs, 0.4 µM forward
184 primer and 0.2 µM bridge primer (primers shown in Table S1), 0.25 µl Phire DNA
185 polymerase (ThermoScientific), and 1/200th of a mosquito gDNA. Reaction
186 conditions were 98°C for 30 sec, followed by 35 cycles of 98°C for 5 sec, 58°C for 20
187 sec, 72°C for 90 sec; followed by a final extension at 72°C for 10 min. The forward
188 primer contained a 5' NheI tag allowing the hairpin RNAi construct to be cloned into
189 pSL-attB-UAS14-gyp[3×P3-eYFP].
190 To synthesize the *cyp4g17* knockdown construct, fusion PCR was carried out to fuse
191 a 517bp region of exon 1 of *cyp4g17* (AGAP000877) and the proceeding 128bp
192 intron (amplified from gDNA), to the reverse complement of the partial exon 1
193 fragment (amplified from cDNA). RNA was extracted from adult G3 females
194 according to Tri Reagent manufacturer's protocol (Sigma) and treated with Turbo
195 DNase (Ambion). First strand cDNA was prepared from approximately 20 ng total
196 RNA using Superscript III First-strand Synthesis System for RT-PCR (Invitrogen).
197 Products from both amplifications were used as template for the final fusion PCR

198 which was then cloned into pSL-attB-UAS14-gyp[3×P3-eYFP] with NheI and NcoI
199 (all primer details in Table S1).

200 ***Transformation of Anopheles gambiae***

201 All *Anopheles gambiae s.s.* mosquitoes were reared under standard conditions and
202 transgenic *attP* RCME docking lines were created by *piggyBac* mediated
203 transformation of the G3 strain with the pBac-CFP using standard procedures (Lynd
204 and Lycett 2012; Lombardo et al. 2009).

205 ***Creation of Gal4 driver lines***

206 Early embryos from transgenic *attP* docking line A14 were injected with buffer
207 containing 350 ng/µl of one of the Gal4Δ, Gal4-FF, Gal4-GFY and native Gal4
208 protein variants of the attB-Hsp Gal4 driver plasmid and 150 ng/µl of intergrase
209 helper plasmid, PKC40, as previously described (Lombardo et al. 2009; Pondeville et
210 al. 2014). Surviving larvae were reared to adulthood and crossed to the G3 strain.
211 G1 progeny were screened for fluorescent eye marker using a Leica MFLZIII
212 microscope fitted with dsRed, YFP and CFP filter sets. Transgenic G1 larvae were
213 pooled according to sex and crossed to the G3 strain. Isofemale lines were obtained
214 from individual female lays and the G2 progeny interbred. DNA extractions and
215 orientation PCR (see below) were carried out on the transgenic G1 parents and lines
216 with a unique transgene cassette arrangement were maintained. A11 Gal4 lines
217 were also generated in similar fashion to test the RCME efficiency using the native
218 Gal4 attB-Hsp Gal4 plasmid.

219 ***Creation of UAS p450 RNAi responder lines***

220 Transgenic UAS responder lines containing the *cyp4g16* and *cyp4g17* RNAi
221 cassettes were made by injection of the A11 embryos with pSL-attB-UAS-

222 cyp16RNAi or pSL-attB-UAS-cyp17RNAi plasmid (350ng/ul) together with the
223 intergrase helper plasmid, PKC40 (150ng/ul) as described previously. G1 larvae
224 positive for eYFP, indicative of an integration event, were used to generate isofemale
225 lines and screened by PCR to determine the orientation of the cassette, as described
226 below.

227 ***Determination of insertion arrangement***

228 A series of four diagnostic PCRs were carried out to determine both the orientation
229 of the *attB* cassettes and, for mosquitoes having both markers, the relative position
230 to the *attP-CFP* cassette, using one external primer and one internal primer (see Fig
231 S3A to describe potential orientations and Table S1 for primers used). DNA from a
232 single G1 adult was extracted using a Qiagen DNeasy Blood & Tissue Kit as per
233 manufacturer's protocol, and DNA eluted in 200µl of ddH_20. PCR was carried out
234 using the manufacturer's recommendations for Phire Hot Start II Polymerase (NEB)
235 using 1 µl of DNA and a final primer concentration of 100nM each, with an annealing
236 temperature of 58°C for 20 seconds, and an extension time of 90 seconds. PCR
237 products were sequenced directly to confirm a precise recombination event at the
238 *attP*/*attB* junction.

239 ***Southern Blots***

240 DNA was extracted from at least 30 male and female adult mosquitoes using Qiagen
241 GenomicTip 20/G columns as described in manufacturer's standard protocol. 9 µg of
242 genomic DNA was then digested to completion with EcoRI (NEB), purified on
243 diatomaceous earth (Carter and Milton 1993) (Sigma) and run on a 0.8% agarose
244 gel. DNA was transferred to a nylon membrane (Lycett et al. 2004). Two probes
245 were amplified from a plasmid template targeting the pBac arms (see Table S1 for

246 primers) and labelled with CTP α-32P 3000Ci/mmol (Perkin Elmer) using Klenow
247 Enzyme (NEB) and random nonamers (Sigma). Hybridization, washing and
248 exposure to X Ray film were performed as described previously (Lycett et al. 2004).
249

250 ***Whole-mount larval abdomen immunostaining.***

251 Abdominal integuments were dissected from 4thinstar larvae and fixed and stained
252 as described previously (Lycett et al. 2006). The rabbit affinity purified CYP4G16 and
253 CYP4G17 antibodies (Ingham et al. 2014; Balabanidou et al. 2016) were used as a
254 1/500 dilution and detected with goat anti-rabbit antibody (Alexa-Fluor 488;
255 Molecular Probes; 1/1,000). Nuclei were stained with ToPRO 3-Iodide (Molecular
256 Probes). Images were obtained on a Leica SP8 confocal microscope.

257 ***Analysis of enhancer trapped gal4 expression***

258 To investigate enhancer driven gal4 expression, crosses were made between the
259 HSP-Gal4 mosquito lines (marked by dsRed) and the UAS mosquito line, Wnd,
260 containing *luciferase* and e*YFPnls* reporter genes (marked by eCFP) (Lynd and
261 Lycett 2012). At least 10 females were used per cross, with at least double the
262 number of males. Larval progeny were screened for expected inheritance of both red
263 and cyan fluorescent eye marker proteins. Adults were examined at three and seven
264 days after emergence. Dissections were carried out using a Leica MFLZ III
265 microscope using YFP, dsRed and CFP filters. Images were taken using an
266 Olympus BX60 microscope fitted with a Nikon DSU2 camera, or through a dissecting
267 microscope fitted with a Nikon P5100 digital camera.

268 ***Luciferase assays***

269 Adult mosquitoes were anesthetized with CO_2 when three to five days old and
270 dissections carried out in PBS. Whole and dissected mosquito larvae and adults
271 were transferred to 200µl of luciferase passive lysis buffer (Promega). Samples were
272 homogenized, and the supernatant used immediately for luciferase assays using a
273 Promega Luciferase Assay Kit (E1500) and a Lumat LB 9507 tube luminometer. At
274 least six replicates for each assay were carried out.

275 ***Investigation of knock down phenotype***

276 Crosses were made between the oenocyte specific Gal4 driver line (DsRed),
277 A14Gal4, and the UAS *cyp4g16* and *cyp4g17* RNAi mosquito lines (YFP) originating
278 from lines carrying integrated hairpin constructs into the *attP* docking site of line A11.
279 Larvae and adults of the resulting progeny carrying both markers, designated 16i
280 and 17i henceforth, were examined for various phenotypes using siblings arising
281 from the same cross without the UAS cassette (dsRed only) as negative controls.

282 ***qRT-PCR of cyp4g16 and cyp4g17***

283 RNA was extracted from different mosquito stages and treated with DNase as
284 above. First strand cDNA was prepared from total RNA using Superscript III First-
285 strand Synthesis System for RT-PCR (Invitrogen). Transcript abundance of the
286 *cyp4g16* and *cyp4g17* genes were examined using two sets of primers for each gene
287 in order to monitor reliability of amplification (details in Table S1). One primer of each
288 pair was designed to span an exon-exon junction. The PCR efficiency, dynamic
289 range and specificity of the primer pair were calculated from running a standard
290 curve over a five-fold dilution series of cDNA. Transcript levels were normalized
291 against amplification of the *An. gambiae* ribosomal protein genes, S7 (AGAP010592)

292 and Ubiquitin (AGAP007927) (Jones et al. 2013). PCR was carried out in a 20 µl
293 reaction volume containing 10 µl Brilliant III SYBR Green Master Mix (Agilent), 500
294 nM of primers, 1µl cDNA (diluted 100-fold). qPCR was performed on the MXPro
295 qPCR system (Agilent) and reaction conditions were 95°C for 10 min followed by 40
296 cycles of 95°C for 10s and 60°C for 10s. Melt curves were performed after each
297 PCR to ensure the specificity of the qPCR. Three technical replicates were run for
298 each sample and a minimum of four biological replicates carried out.

299 ***Western Blots***

300 Early pupae (less than 2hours old) were extracted in 1x Laemlli buffer (BioRad) with
301 100mM DTT. Proteins were separated on 10% SDS-PAGE with a Tris-glycine
302 running buffer (192 mM glycine 25 mM Tris, 0.1% SDS) and transferred to
303 polyvinylidene fluoride (PVDF) membrane. Filters were blocked with 3% powdered
304 milk in PBST (PBS+0.1% Tween-20) for 1h at room temperature and then incubated
305 with anti-CYP4G16 (1:200 dilution (Balabanidou et al. 2016)), anti-CYP4G17 (1:200
306 (Ingham et al. 2014)) or anti-alpha tubulin (1:500 Sigma) antibodies in 3% milk-PBST
307 for 1 h at room temperature. Membranes were washed four times in PBST for 5 min,
308 then incubated with anti-rabbit (1:40,000) or anti-mouse (1:10,000) secondary
309 antibodies conjugated to peroxidase. Filters were developed with the Western blot
310 Chemiluminescence Reagent Plus Kit (Renaissance) and exposed to X-ray films.
311

312 ***Gas chromatography-mass spectrometry analysis***

313 Cuticular hydrocarbons of single 16i and 17i one day old female adults or female
314 pupae collected within 5 hours of larval/pupal transition, together with identically
315 reared sibling A14Gal4:+ mosquitoes, were extracted by a 5 minute immersion, with
316 gentle agitation at room temp, in 50 µl hexane (Sigma-Aldrich) containing 10 ng/µl

317 octadecane (Sigma-Aldrich) internal standard. Hydrocarbon identification and
318 quantification was performed by gas chromatography-mass spectrometry (GC-MS).
319 The mass spectrometer employed was a Waters GCT and the GC column was a 30
320 cm long, 0.25 mm internal diameter, 0.25 μm film thickness BPX5 (SGE). The oven
321 temperature gradient was 70°C to 370°C at 10°C/minute and the carrier gas was
322 helium (BOC) at a flow rate of 1 ml/minute. The injection volume was 1 μl. The MS
323 scan range was *m/z* 40 to 450 Da in scan time 0.6 s. Peak identification was by a
324 combination of retention time, library searches using the NIST mass spectrum library
325 supplied with the instrument and reference to published spectra. Peak areas were
326 measured manually using the peak integration tool in the Waters Mass Lynx
327 software. A representative annotated trace is provided in File S1. The total amount of
328 hydrocarbon present was calculated by summing all of the peak areas detected
329 relative to the internal standard. Statistical analysis of total CHC was performed by
330 ANOVA with Tukey HSD correction. The relative quantity of individual hydrocarbons
331 present in each mosquito sample were compared in two ways. 1) relative to the
332 internal standard, by dividing the area of each extracted hydrocarbon peak to that of
333 the internal standard to give a quantitative value to each hydrocarbon and 2) relative
334 to the total hydrocarbon content in each mosquito by dividing each area by the sum
335 of all areas to give a fraction of the total (statistical analysis provided in File S2 and
336 File S3 for normalization against Internal Standard and total CHC respectively).

337 ***Desiccation Assays***

338 10-13 mosquitoes aged two to five days were placed in 70 ml transparent
339 polystyrene pots and a netting mesh lid attached with an elastic band. Pots were
340 then placed in 300 ml transparent polystyrene desiccation chambers with 10g silica
341 gel desiccant, sealed with a screw on cap and placed in a 32°C incubator. Desiccant

342 is thought to reduce humidity to < 10%, (Gray and Bradley 2005). 7 replicates for 16i
343 and A14A1 sibling females, and 6 replicates for 16i and A14A1 sibling males were
344 performed. Survival was measured by the ability to stand, cling to walls or fly and
345 was scored at the indicated times. Statistical analysis was performed by Cox
346 regression.
347
348 **Data and Reagent Policy**
349 All extant mosquito lines and novel plasmids described in the manuscript are
350 available for distribution. Supplementary data deposited at Figshare includes
351 Schematic of the constructs used for transformation Figure S1, Summary of
352 generation of docking lines Figure S2, Phenotypic characterisation of RCME lines
353 Figure S3, Dissection of Female Adult and Pupa derived from A14Gal4 x UAS-
354 mcherry cross Figure S4 Images of A11Gal4 X UAS-nlsYFP progeny Figure S5
355 CYPG16 and CYP4G17 larval expression Figure S6, Schematic of the constructs
356 used for gene knockout Figure S7, Western analysis of 16i,17i and A14A1 early
357 pupae, Figure S8, Plots of relative abundance of CHCs with respect to internal
358 standard Figure S9, Plots of relative abundance of CHCs with respect to total CHC
359 Figure S10. Sequences of primers described in Materials and Methods Table S1,
360 Summary table of RCME experiments performed with different Gal4 constructs in
361 A14 docking line Table S2, Representative, annotated GCMS CHC trace from
362 individual mosquitoes File S1, Statistical analysis of CHC normalized to Internal
363 standard File S2, Statistical analysis of CHC normalized to Total CHC content File
364 S3.
365
366

367

368 **Results**

369 **Generation of oenocyte driver line**

370 ***Oenocyte expression in docking line A14***

371 We created a series of *piggyBac* based PhiC31 docking strains of *An. gambiae*,
372 carrying inverted *attP* sites flanking the cyan fluorescent protein (*eCFP*) selectable
373 marker and the *LRIM*1 (Povelones et al. 2009) gene controlled by the blood meal
374 inducible Vitellogenin promoter (Chen et al. 2008)(Fig S1A). From 10 isofemale lines
375 produced (Fig S2A), four carried insertions into single genomic sites, as indicated by
376 inverse PCR (Fig S2B). All lines had the expected expression of eCFP in eyes and
377 neuronal tissues, and six out of eight examined expressed the tagged *LRIM1*
378 transcript (Fig S2C) 48hrs after bloodfeeding. Western analysis indicated that three
379 insertion lines with single copy insertions, A11, A14 and BB57, expressed the tagged
380 LRIM1 protein after bloodfeeding (Fig S2D).

381 However in one line, A14, distinct eCFP fluorescence was also readily detected in
382 oenocytes in larval and pupal stages (Fig 1), suggesting that one or more local
383 genomic enhancers were directing eCFP expression to these abdominal cells.
384 Sequencing around the transposon insertion site in A14, indicated that integration
385 had occurred at an intergenic site on the 3R chromosome (Fig S2E), greater than
386 30Kb away from the nearest annotated gene in the PEST genome (Vectorbase
387 P4.12). Since we created the A14 line to carry inverted *attP* sites surrounding the
388 marker and effector cassette, we surmised that recombinase-mediated cassette

389 exchange (RCME) with a promoterless Gal4 construct would bring the transctivator
390 under control of the enhancer to produce oenocyte specific driver lines.

391 **RCME is efficient in mosquitoes**

392 To initially develop an efficient oenocyte driver, we examined the efficacy of four
393 alternative Gal4 constructs marked with dsRed, by targeting cassette exchange into
394 A14 embryos. Previous cell culture analysis indicated that these alternative Gal4
395 constructs, native Gal4, Gal4-delta, Gal4-GFY and Gal4-FF generate different
396 transcriptional activation potentials (Lynd and Lycett 2011), and so may produce a
397 graded range of oenocyte-specific expression levels. As indicated (Table S2),
398 between 6 and 155 dsred positive larval progeny were successfully generated for
399 each construct. However, viable adults were only obtained using the native Gal4
400 (>100 adults) and Gal4-FF (1 adult from 6 dsred positive F1 larvae) transactivators.

401 Should canonical cassette exchange of the dsred marked Gal4 driver have occurred
402 in the eCFP marked A14 line, the red marker would replace the blue marker, in two
403 potential orientations. Whereas integration into a single *attP* site, in four possible
404 orientations, would conserve the *eCFP* marker in this locus, and thus F1 progeny
405 would be doubly marked (this is illustrated in Fig S3A). In total seven isofemale
406 native Gal4 lines were bred from surviving F1 progeny; three exchange and four
407 integration lines. PCR analysis indicated that five of the six possible integration
408 patterns were detected within these lines (Table S2). Southern hybridization on the
409 representative A14Gal4 line (A1 line kept for further characterisation) confirmed
410 cassette exchange into the expected genomic site and orientation (Fig 2A and B).

411 Since RCME efficiency had not previously been assayed in mosquitoes, we also
412 tested a second control docking line, A11, that displayed the typical expression of

413 the 3xP3 marker. Into the A11 line we exchanged the same native Gal4 construct
414 and obtained 21 isofemale lines from 638 embryos injected. Diagnostic PCR was
415 again used to define orientation of insertion in six of these lines (Table S2) and
416 Southern blotting of an A orientation isofemale line confirmed that RCME had
417 occurred at the expected site due to the expected change in restriction enzyme
418 pattern (Fig 2A and B) compared the parental line.

419 **Oenocyte enhancer is trapped by RCME.**

420 In the A14 native Gal4 trap lines, weak red fluorescence was detected in oenocytes
421 following exchange in the A14A1 and A14A2 lines (Fig S3B). To examine whether
422 Gal4 expression was also under oenocyte enhancer control, the A14 Gal trap lines
423 with alternative orientations of insertion (including alternative isofemale lines with the
424 same molecular orientation, A14A1 and A14A2) were crossed to a 3xP3 *CFP*
425 marked responder line carrying nuclear localised yellow fluorescent protein (nlsYFP)
426 and luciferase genes both under control of the upstream activation sequence (UAS),
427 to allow qualitative and quantitative analysis, respectively (Lynd and Lycett 2012). In
428 progeny of these crosses, nlsYFP was visible in larval (Fig 3B), pupal and adult
429 oenocytes (Fig 3D), indicating that enhancer trapping was achieved. Furthermore,
430 through Gal4 enhanced expression we could trace the development of adult
431 oenocytes through 4th instar larval (Fig 3F) and pupal stages as they contained
432 nlsYFP. The same oenocyte expression profile was obtained in progeny following
433 A14Gal4A crossing with a separate UAS-mCherry line (Adolfi et al. 2018) (Fig S4).
434 Progeny from crosses between the A11Gal4A line with the UAS-nlsYFP line are
435 shown in Fig S5 and lack expression in the oenocytes.

436 Quantitative analysis of the different orientation A14Gal4 lines (Table S2) by
437 luciferase activity analysis indicated that in both 4th instar larvae and adults, the
438 cassette orientation (Fig S3A) had a significant effect on reporter gene expression.
439 Those with orientation A had three-fold more activity than those with orientation B at
440 larval stages (Fig S3C), and nine-fold greater expression at adult stage (Fig S3D).
441 Further analysis of the A14A1 line indicated that luciferase activity increases 100-fold
442 during larval development, plateaus during metamorphosis, before dropping four-fold
443 in adult stages (Fig S3E).

444 **Expression of 4Gs in immature stages**

445 To examine the utility of the driver line for oenocyte-specific knockdown of CHC
446 regulating enzymes, we targeted two genes, *cyp4g16* and *cyp4g17*, that previous
447 work had established were highly expressed in adult oenocytes (Ingham et al. 2014;
448 Balabanidou et al. 2016). To determine the expression profile of native mosquito
449 *cyp4g*s in immature stages, we performed qPCR analysis on RNA extracts from
450 larval and pupal samples collected at defined timepoints following moulting. *cyp4g16*
451 was shown to be highly transcribed relative to housekeeping gene controls (delta C^T:
452 Fig 4A) throughout the 3rd instar and significantly increased (up to eight-fold) during
453 4th instar and pupal stages (Fig 4A). Whereas the *cyp4g17* transcript was at the
454 minimal limits of detection in 3rd instar stages, and expression massively increased
455 (up to 10,000-fold) after 8 hours of the early 4th instar stage, before decreasing
456 during pupal moult, and again increasing significantly at later pupal stages (Fig 4B).
457 Immunostaining confirmed that both CYP4G proteins are readily detected in 4th
458 instar larval oenocytes. (Fig S6 A,B).

459 **Oenocyte Gal4-driven knockdown of *cyp4g16* or *cyp4g17* produces different**
460 **survival phenotypes**

461 UAS responder constructs were created carrying inverted repeats of DNA from each
462 *Cyp4g* gene, separated by their natural intron sequences, as shown in Fig S7. These
463 were exchanged by RCME into the control A11 *attP* line, and distinct eYFP
464 isofemale responder lines carrying insertions of UAS-*Cyp4g16* and UAS-*Cyp4g17*
465 hairpins in the same orientation were generated. No deleterious phenotype has been
466 observed in these lines and they have been maintained in colony for 4 years since
467 production.

468 However, following crossing to the A14 driver line, the resultant transheterozygote
469 progeny undergo death at distinct pupal stages depending on the specific RNAi
470 construct present. Progeny expressing *cyp4g16* RNAi in oenocytes (16i) show high
471 mortality (above 90%) at early-mid pupal stages (Fig 5 A), which is reduced if grown
472 at low density (<200 larvae in a 30x30x5cm tray - in a typical experiment we
473 observed around 60% death at early pupal stage, Table S3). The progeny
474 expressing *cyp4g17* RNAi in oenocytes (17i) develop till late pupal stage and have
475 high mortality (>90%) in pharate adults or as the adults emerge from the pupal case
476 (Fig 5B, Table S3). Altering growth conditions does not increase 17i survival.
477 Homozygous A11 and sibling heterozygous A14Gal4 mosquitoes typically show
478 greater than 90% survival during 4th instar larval to adult transition (Table S3).

479 **Stable RNAi efficiently knocks down expression of *cyp4g* genes.**

480 To examine efficiency of knock down of the *cyp4g* genes, western analysis and
481 qPCR was performed on early pupae prior to death in 16i and 17i mosquitoes.
482 Western analysis revealed an absence of CYP4G16 in 16i mosquitoes (Fig 5C).

483 Similarly, the major protein corresponding to CYP4G17 was absent in 17i pupal
484 extracts (Fig 5D). In concordance with lack of protein, transcript levels were reduced
485 by 90% in both knockdowns relative to Gal4 driver line, A14 (Fig 5E). Western
486 analysis also indicated that knock down was specific to the respective CYP4G
487 proteins, since the level of CYP4G16 was similar to controls in 17i knockdown
488 mosquitoes, and *vice versa* (Fig S8).

489 **CYP4G16 and CYP4G17 have a synergistic role in CHC synthesis in pre adult**
490 **stages**

491 Total CHC analysis of early pupae hexane cuticle extracts by gas chromatography–
492 mass spectrometry (GC-MS) demonstrated that 16i or 17i mosquitoes both had a
493 significant reduction of approximately 80% compared to controls (Fig 6A). Whereas,
494 in surviving adults, this reduction in total CHC content was approximately 50% in
495 both knockdowns (Fig 6B). However, there was no significant difference in total CHC
496 between the 16i and 17i mosquitoes at either stage.

497 Separating the analysis down to the relative peak areas of individual hydrocarbons
498 (with respect to the internal standard), no CHC species showed a significant
499 difference (File S2) in abundance between the 16i and 17i knockdowns at the early
500 pupal stage (Fig S9). In contrast, all individual CHCs (except nonadecane) were
501 significantly reduced ($p<0.05$) in 17i pupae compared with controls (Fig S9). Most
502 CHCs were also significantly reduced in 16i pupae compared to controls, although
503 nonadecane $p=0.55$, icosane $p=0.08$, triacontane $p=0.56$ and hentriacontane $p=0.08$
504 were exceptions. At the adult stage, nonadecane was significantly reduced in 16i
505 mosquitoes compared to 17i, whereas methyl-hentriacontane was significantly
506 reduced in 17i compared to 16i mosquitoes. The major adult peaks, penta-, hepta-

507 and nona-cosane were significantly reduced in both 16i and 17i mosquitoes
508 compared to controls, as were hexacosane and hentriacontane. Additional significant
509 differences between 17i and control mosquitoes were observed with octacosane,
510 and methyl-nonacontane and methyl-hentriacontane (Fig S9).

511 Analysis of the relative proportion that individual CHCs comprise of total CHC
512 content indicate that in control pupa, four odd-number chain alkanes provide over
513 70% of all hydrocarbons (henicosane 22%, tricosane 15%, pentacosane 17.5%,
514 heptacosane 18%) (Fig S10). The relative proportions of all four major CHCs are
515 significantly reduced ($p<0.05$) in both 16i and 17i pupae compared to controls (File
516 S3). In addition, whilst the relative proportion of the two methyl branched chain
517 CHCs (methyl-nonacosane and methyl-hentriacontane) are also reduced in 16i
518 pupae ($p<0.01$, $p<0.001$), only the latter ($p<0.01$) is also reduced in 17i pupae
519 compared to controls. Contrastingly, nearly all of the other minor peaks show
520 significant relative increase in the 16i and 17i knockdown pupae compared to
521 controls. When directly comparing the two knockdown mosquitoes, the relative
522 proportion of hepta- and nona-cosane and the two methyl branched chains are
523 significantly lower in 16i, whereas octacosane and tricontane are significantly lower
524 in 17i pupae than 16i.

525 In control adults, there is a shift to higher molecular weight CHCs compared to
526 control pupa with two odd chain alkanes providing over 50% of all hydrocarbons
527 (heptacosane 35%, nonacosane 19%). In 16i knockdowns, both of these CHCs are
528 significantly reduced in relative proportion compared to control. Whereas
529 heptacosane and methyl-hentriacontane are significantly lower in 17i mosquitoes
530 compared to control. Again the majority of the minor peaks show increases in
531 relative abundance in both knockdowns. Comparison of the 16i and 17i knockdowns

532 indicated that nonadecane and nonacosane were significantly reduced in 16i
533 knockdowns, whereas methyl-hentriacontane ($p<0.001$) was significantly reduced in
534 17i knockdown. There was also a non significant trend ($p=0.06$) in relative reduction
535 in methyl-nonacosane in the 17i knockdown.

536 ***cyp4g16* knockdown increases susceptibility to desiccation.**

537 Due to the high mortality in 17i pharate adults, the effect of CYP4G depletion on
538 desiccation tolerance was only assessed in 16i adults. The time course of survival of
539 16i males and 16i females versus co-reared, age matched, sibling Gal4 controls
540 when exposed to a low humidity environment is illustrated in Fig 5C and Fig 5D,
541 respectively. Cox proportional hazards analysis of the time to mortality data was
542 initially fit to a model comprised of three terms, for sex, genotype, and sex by
543 genotype interaction effects, respectively. The interaction term was found to be non-
544 significant so was removed from the model. This analysis suggested highly
545 significant effects of both sex ($p < 0.001$) and genotype ($p < 0.001$) on the risk of
546 death. In other words, males show significantly different survival to desiccation
547 compared to females, and gene knockdown has a significant effect on survival time
548 irrespective of sex. Moreover, analysis of individual sexes, males and females
549 indicated that both 16i males ($p < 0.001$) and 16i females ($p < 0.001$) were
550 significantly more sensitive to desiccation than their respective same sex controls.

551

552 **Discussion**

553 Following serendipitous detection of oenocyte-specific fluorescence in one of a panel
554 of RCME docking lines, we have successfully performed Gal4 based enhancer

555 trapping in *An.gambiae* for the first time. Previous work has shown that enhancer
556 trapping was feasible in mosquitoes through mobilisation of tagged transposable
557 elements, and the subsequent changes in tissue specific expression of reporter
558 genes (O'Brochta et al. 2011). Further work by this group developed enhancer
559 trapping (O'Brochta et al. 2012) and more recently large scale promoter/gene traps
560 in *An. stephensi* (Reid et al. 2018). We have taken a modified approach through the
561 use of RMCE to insert alternative Gal4 genes nearby a putative enhancer. Although
562 there is, as yet, no annotation for a gene closer than 30kb from the A14 insertion
563 site, oenocyte-specific regulation is achieved by cassette exchange demonstrating
564 that the locus contains DNA regions which interact with the minimal promoter
565 present on the Gal4 driver. The work has thus confirmed that RCME is efficient in
566 *An. gambiae* (Hammond et al. 2016). We have also generated a docking line, A11,
567 into which RCME and subsequent Gal4 dependent gene silencing phenotypes were
568 demonstrated with UAS-regulated hairpin RNAi constructs.

569 To develop the oenocyte driver, we assessed four variants of Gal4, each carrying
570 alternative transactivators. These were shown previously to have graded activation
571 potentials with Gal4Δ> GFY > Gal4 > FF in transfected *An. gambiae* cells (Lynd and
572 Lycett 2011). In these cells, the relative activation potential varied 20-fold between
573 the four transactivators, with Gal4Δ being 10-fold more active than Gal4. RCME
574 derived dsred positive G1 larvae were obtained with each construct, but only those
575 generated with native Gal4 transactivator surviving in large numbers to the adult
576 stage, with the majority of those derived from Gal4Δ and GFY dying at early larval
577 instar. This is in contrast to previous work with GFY combined with a gut specific
578 carboxypeptidase promoter which gave very high transformation rates and robust
579 homozygous adults that are still in colony (Lynd and Lycett 2012). This would

580 suggest that the higher transactivation potential of modified Gal4s show toxicity in
581 mosquitoes when expressed from the oenocyte enhancer, presumably through a
582 'squelching' process (Gill and Ptashne 1988). The efficiency of precise cassette
583 exchange with the A14 and A11 lines would appear to be at least 1 in 50 to 100
584 embryos injected, and thus similar to *piggyBac* transformation rates in this lab (Lynd
585 and Lycett 2012; Lycett et al. 2012; Lombardo et al. 2009)

586 By assaying luciferase expression in crosses between a UAS responder line and
587 alternative RCME lines that had the Gal4 cassette inserted in opposite orientations
588 with respect to the *piggyBac* arms, we observed that relative activation potential was
589 significantly higher when the Gal4 was inserted nearer to the right *piggyBac* arm (i.e.
590 Orientations A > B Fig S3) in both larvae and adults. However, significant activation
591 was detected in both orientations, as would be predicted from a local enhancer that
592 acts upstream or downstream of a target gene (Khoury and Gruss 1983).

593 By fluorescently tagging both larval and adult oenocytes, we are able to visually
594 follow the development of adult oenocytes during the 4th instar to adult stage, with
595 the parallel loss of larval oenocytes during late pupation. The timing of the mosquito
596 oenocyte cell development pathways has been documented as early as 1960
597 (Christophers 1960), but generating a Gal4 driver for these cells has opened the
598 possibility for a variety of cellular and functional analysis. For example, this tagging
599 will enable isolation of pure cells for 'omics' analysis; however, initially we have used
600 the oenocyte driver to examine the *in vivo* function of two CYP4G P450s annotated
601 in *An. gambiae*.

602 Our previous *in vitro* analysis could only detect aldehyde decarbonylase activity for
603 recombinant CYP4G16 when assayed with a C18 substrate, yet both genes are

604 highly expressed in pupal and adult oenocytes, implicating both for roles in this cell
605 type (Ingham et al. 2014; Balabanidou et al. 2016; Kefi et al. 2019). Furthermore,
606 here extending immunolocalisation analysis of the abdomen integument to an earlier
607 stage shows that both genes are also expressed in 4th instar larval oenocytes, yet
608 qPCR shows distinct temporal transcription patterns. *cyp4g16* is highly constitutively
609 expressed throughout all life stages examined, and only increases 10-fold during 4th
610 instar and pupal stages compared to the 3rd instar, whereas *cyp4g17* is barely
611 detectable in 3rd instar larvae, but is very highly induced in 4th instar and late pupal
612 stages (up to 10,000-fold). The temporal profiles would suggest that the two genes
613 have distinct roles in *An. gambiae* related to life cycle stage, which correlates with
614 the early and late onset of lethal pupal phenotypes observed in the RNAi
615 knockdowns. It may also indicate that the expression of the two genes are regulated
616 by different effectors. The regulation of cyp4G17 in 4th instar larvae and pupae would
617 suggest control linked to larval to adult transition, perhaps hormonal.

618 As female *An. gambiae* age there a relative decrease in abundance of low molecular
619 weight (LMW) CHCs (up to heptacosane) and an increase in the relative abundance
620 of higher MW CHCs including heptacosane, nonacosane, hentriacontane and
621 methyl-hentriacontane (Caputo et al. 2005), which is recapitulated in the CHC
622 analysis performed on pupal and adult stages here, and most clearly seen in the
623 controls samples in Fig S10. When examining total CHC content in early pupae and
624 surviving one day old adults it was clear that silencing either gene results in a similar
625 80% and 50% reduction respectively. Most strikingly, both gene knockouts have a
626 significant reduction in abundance of nearly all CHCs at the pupal stage compared
627 with the control, however no significant difference in abundance of individual CHCs
628 between the two knockdowns were detected at this stage. Which would indicate both

629 enzymes have major roles in CHC synthesis *in vivo* and have significant overlapping
630 substrate specificity. The fact that both individual knockdowns produce 80%
631 reductions in total pupal CHC also suggests a degree of synergism in CYP4G
632 activity in 4th instar larvae and pupae.

633 Significant differences in the two knockdowns were observed however when
634 analysing relative abundance of each CHC compared with the total CHC content.
635 The 16i knockdowns pupa had relatively less of the major HMW alkanes and methyl-
636 alkanes compared with 17i knockdowns, whereas 17i had significantly lower ratios of
637 the minor even-chain CHCs. The lower proportion of higher molecular weight CHCs
638 would suggest that the earlier larval expression of *cyp4G16* is critical for generating
639 the appropriate relative abundance of CHCs for early pupal survival, and the relative
640 ratio of CHCs may be a contributing factor to the death observed in the early 16i
641 pupae.

642 The CHC profiles from adults have to be addressed with the caveat that since the
643 adults we analysed are outliers which have survived eclosion, and may well have
644 less extreme changes than those which die and were excluded. Despite this, in the
645 adult survivors, there is evidence of small differences in absolute CHC content
646 between the knockdowns, in that *cyp4g16* knockdown adults show reduced levels of
647 nonadecane compared with 17i individuals, whilst *cyp4g17* knockdowns show
648 reduced levels of methyl-hentriacontane compared to *cyp4g16* knockdowns. The
649 differences observed between 16i and 17i in relative proportion of individual CHC
650 compared to total CHC were less pronounced in the adult than in the pupae, which
651 may be a reflection of outlier analysis. In adults, nonadecane and nonacosane were
652 reduced in 16i and, opposite to the pupal data, the HMW methyl-CHCs were
653 relatively reduced in 17i compared to 16i. Indicative of an enhanced role for

654 CYP4G17 in generating methyl-CHCs late in pupal development that perhaps
655 facilitates the eclosion process.

656 The CHC profiling would thus suggest that the two enzymes have significant overlap
657 of substrate specificity, and at the early pupal stage the enzymes work
658 synergistically. At this stage, the CYP4G16 has been active since at least 3rd instar
659 and has slight dominance in the production of HMW CHCs. During later pupal to
660 adult development, CYP4G17 appears dominate in the production of methyl
661 branched chains. A propensity to generate methyl-CHCs was also observed when
662 *cyp4g17* is ectopically expressed in cyp4G1 silenced in Drosophila (Kefi et al, 2019).
663 It should be noted however that the temporal analysis is complicated by the unknown
664 rate of deposition of internally stored CHCs to the cuticle. Furthermore, the effect of
665 observed changes in sub-cellular localisation of the CYP4Gs at different
666 developmental stages may play a role in enzyme activity. At the 4th larval stage, we
667 have previously shown both enzymes are localized in the periphery of the oenocyte
668 cell membrane (Kefi et al. 2019), where synergistic function may be facilitated. In the
669 developing adult oenocytes cyp4G16 maintains its peripheral cell localisation,
670 whereas cyp4G17 was observed to localise more broadly throughout the
671 endoplasmic reticulum (Kefi et al. 2019), which may alter which substrates the two
672 enzymes encounter and their subsequent activities.

673 All insects possess one or more *cyp4g* P450s (phylogenetic tree in (Calla et al.
674 2018). In *D. melanogaster* their two annotated genes have distinct tissue specific
675 expression patterns, although only *DmCyp4g1* is expressed in oenocytes throughout
676 life and has a critical role in CHC production (Qui et al. 2012), whereas *cyp4g15*
677 appears predominantly neuronal and of ill-defined function (Maibeche-Coisne et al.
678 2000). Oenocyte-specific *Dmcyp4g1* RNAi knockdown produces a temporally similar,

679 partially incomplete, lethal pharate adult phenotype similar to that observed in
680 *cyp4g17* knockdown mosquitoes. Although the mortality during eclosion of the vast
681 majority of 17i mosquitoes precluded analysis of desiccation tolerance, the most
682 parsimonious explanation for pharate adult death is severe desiccation intolerance.
683 However, we cannot rule out other developmental irregularities, including a direct or
684 indirect role for CHCs to facilitate escape from the pupal cuticle (Chiang et al. 2016).
685 The more weakly penetrant lethal phenotype in *cyp4g16* knockdown pupae, allowed
686 the demonstration of significant sensitivity to desiccation in surviving adults. This
687 supports the hypothesis that a primary determinant of desiccation tolerance in
688 *Anopheles* mosquitoes is total CHC content (Arcaz et al. 2016). This later study also
689 demonstrated a positive correlation between octacosane and desiccation tolerance
690 that was significantly depleted in the *cyp4g17* knockdown mosquitoes.

691 Transient knockdown of the single *cyp4gs* in holometabolous locusts (Yu et al. 2016)
692 and pea aphids (Chen et al. 2016) also produce a desiccation sensitive phenotype.
693 In the former case, the lethal phenotype could be rescued by maintenance at 90%
694 humidity. However, attempts to rescue *cyp4g17* knockdown mosquitoes was
695 unsuccessful when maintained at close to 100% during eclosion (not shown).

696 Although this is the first time that two *cyp4g*s have both been shown to be essential
697 for CHC production in an insect, *in vitro* activity of recombinant proteins from the two
698 annotated *cyp4g*s from the Mountain Pine beetle both convert long chain alcohols
699 and aldehydes into HCs (MacLean et al. 2018). This led to speculation that one or
700 both may be involved in CHC and pheromone production. However, their *in vivo*
701 function and anatomical distribution is yet to be explored in this beetle. In this
702 context, the finding that the single CYP4G from honey bees, that also
703 decarbonylates aldehydes (Calla et al. 2018), is located in antennae and other

704 chemosensory organs (Mao et al. 2015; Calla et al. 2018), as well as abdominal
705 tergites associated with wax production, may suggest a second role in
706 chemoreception for this P450 class. Further work will be needed in Anopheles
707 mosquitoes to examine the functional role of *cyp4g* expression in sensory organs,
708 since data from RNA-Seq (Pitts et al. 2011), indicate significant transcription of both
709 *cyp4g16* and *cyp4g17* in *An. gambiae* antennae.

710 In summary, successful enhancer trapping of oenocyte regulatory regions by RMCE,
711 and the subsequent use of stable RNAi have enabled us to examine the role of two
712 highly expressed CYPs in CHC production and paved the way for in depth analysis
713 of the metabolic roles of oenocytes in mosquitoes. For example, the driver line will
714 be critical for oenocyte-specific gene knockdown and ectopic over-expression to
715 examine the complex metabolic functions of these cells in the malaria mosquito, and
716 to explore their potential role in pheromone production, mating behaviour and
717 longevity (Joseph et al. 2018; Combs et al. 2018).

718 **Acknowledgements**

719 We'd like to thank Amalia Anthousi for great technical assistance in mosquito
720 husbandry and Dolphine Amenya for her major role in the initial generation and
721 characterisation of the pBac-CFP lines. We also thanks Jacob Chapman and Judit
722 Bagi for assistance with qRT-PCR analysis. We also are indebted to Mark Prescott
723 and Rob Beynon who performed the CHC analysis at the Centre for Proteome
724 Research, University of Liverpool, Mike Povelones for providing LRIM1 clones and
725 antibodies, Leonie Ringrose for the PKC40 plasmid, and to Hilary Ranson for
726 thoughtful comments on the manuscript. We are also extremely grateful for two
727 anonymous reviewers that greatly improved the manuscript. The work was partly
728 funded by the EU FP7 Avecnet Grant ID: 265660.

729

730

731 **FIGURE LEGENDS**

732 Figure 1 Oenocyte-specific expression of ECFP marker in A14 larvae and pupa

733 Oenocyte-specific expression of eCFP in larva and pupa in docking line A14
734 presumably caused by a local oenocyte enhancer near to pBac-CFP [attP-LRIM1]
735 integration site. Upper figures are bright field images and lower figures are images
736 taken through CFP filter on stereofluorescent microscope. LO indicates larval
737 oencoyctes which persist during young pupae. ECFP expression in eyes and ventral
738 nerve cord are characteristic of 3xP3 expression.

739 Figure 2 Schematic of *piggyBac* and RCME genomic integrations and Southern
740 analysis

741 A: Schematic of PBac-CFP [attP-LRIM1] integrated by RMCE into genomic DNA of
742 A14 and A11 lines and orientation of exchanged attB HSP-Gal4 cassettes. ****,
743 pBAC L and pBAC R probes; E, EcoRI restriction site; Paired black triangles, *attP*
744 sites; mixed black and white paired triangles, attL and attR sites resulting from
745 phiC31-mediated recombination. Distance from pBac integration sites to flanking
746 genomic EcoRI sites were estimated from the Southern blot as A11 3.0Kb and
747 3.7Kb, A14 1.2Kb and 7.7Kb. B: Southern blot showing single copy integration (two
748 probes – two bands) and shift in expected size of hybridizing fragments following
749 exchange of attB HSP-Gal4 into A11 and A14 genomic sites.

750 Figure 3 Oenocyte Enhancer trapping in larval and adult oenocytes

751 Images of yellow nuclear florescence in progeny of crosses between A14Gal4 driver
752 line and the UAS responder line containing *eYFPnls* reporter genes. A and B; show
753 YFP expression in the oenocytes located in the abdomen of 3rd instar larvae. C and
754 D; show bright field and fluorescent images of the dissected adult abdomen
755 integument. YFP expression is visible in the larval oenocytes (LO) and adult
756 oenocytes (AO). E and F show bright field and fluorescent images of 4th instar larvae
757 showing the development of adult oenocytes on the ventral side of the integument.

758 Figure 4 QRT-PCR analysis of *cyp4g16* and *cyp4g17* during larval and pupal stages

759 Lower graphs show mean delta C^T differences in expression compared to the
760 housekeeping controls to clearly demonstrate the higher constitutive expression of
761 *cyp4g16* in earlier stages, with error bars indicating standard error of the mean.
762 Upper graphs are transformed C^T data that shows the relative fold change in
763 expression (delta delta C^T) at each stage compared to newly moulted 3rd instar
764 larvae to demonstrate the large relative induction of *cyp4g17* expression at later
765 stages. Assays were performed in triplicate on four independent samples. 3 refers to
766 newly moulted 3rd instar larvae, 3.8: 3rd instar larvae aged 8 hours from moult, 3.16:
767 16 hours from moult, 4: newly moulted 4rd instar larvae, 4.8 4rd instar larvae aged 8
768 hours from moult, 4.16 16 hours from moult, P0: newly moulted pupa, P16: Pupa 16
769 hours from moult, P24: Pupa 24 hours from moult. Statistical analysis is performed
770 on C^T data and those values sharing letters do not show significant difference
771 between themselves at $p<0.05$ cutoff by Welch test. The fold change data is simply
772 transformed C^T data and statistical analysis should be taken from the raw C^T data.

773 Figure 5 Analysis of 16i and 17i knockdown efficiency and lethality phenotype

774 A and B Images displaying the different temporal pupal phenotype deaths occuring
775 with 16i and 17i knockdown mosquitoes respectively. A: 16i pupae have a high
776 mortality at early pupal stage characterised by sinking in water (right) and elongation
777 of the pupae (left) at death rather than the characteristic comma shape. B: 17i death
778 is characterized by very late pupal death (left) usually after the pupal case is cleaved
779 at eclosion or during adult emergence (right). C and D: upper western analysis of
780 knockdown of CYP4G16 in 16i mosquitoes and of CYP4G17 in 17i mosquitoes using
781 the respective polyclonal antibodies. C and D: lower loading control of same filters
782 probed with anti-alpha tubulin antibody. E: Analysis of transcript knockdown of the
783 respective *cyp4g* by qRT-PCR analysis of *cyp4g16* and *cyp4g17* in 16i and 17i
784 pupae compared with A14Gal4 (normalized to 1) sibling control mosquitoes that
785 carried the oenocyte driver but lack the UAS-hairpin constructs.

786 Figure 6 Total CHC content in female 16i and 17i mosquitoes and desiccation
787 tolerance of 16i males and females.

788 A: histogram illustrating total CHC content of female pupae collected within 5 hours
789 of larval/pupal transition. B: histogram illustrating total CHC content of one day old
790 female adults. Black bars indicate the median total CHC content per mosquito, black
791 circles are values per mosquito. Boxes are 25th and 75th percentiles and whiskers +
792 and – 1.5 x interquartile range. *** $P<0.001$ calculated by ANOVA followed by
793 Tukey's HSD (Honestly Significant Difference) for pairwise comparisons. C and D:
794 survival curves for 16i and A14Gal4 male (C) and female (D) mosquitoes exposed to
795 low humidity. Statistical analysis performed by Cox regression (Analysis and P
796 values indicated in results text).

797

798 Adolfi, A., E. Pondeville, A. Lynd, C. Bourgouin, and G.J. Lycett, 2018 Multi-tissue
799 GAL4-mediated gene expression in all Anopheles gambiae life stages using
800 an endogenous polyubiquitin promoter. *Insect Biochem Mol Biol* 96:1-9.
801 Arcaz, A.C., D.L. Huestis, A. Dao, A.S. Yaro, M. Diallo *et al.*, 2016 Desiccation
802 tolerance in Anopheles coluzzii: the effects of spiracle size and cuticular
803 hydrocarbons. *J Exp Biol* 219 (Pt 11):1675-1688.
804 Balabanidou, V., A. Kampouraki, M. MacLean, G.J. Blomquist, C. Tittiger *et al.*, 2016
805 Cytochrome P450 associated with insecticide resistance catalyzes cuticular
806 hydrocarbon production in Anopheles gambiae. *Proc Natl Acad Sci U S A* 113
807 (33):9268-9273.
808 Barolo, S., L.A. Carver, and J.W. Posakony, 2000 GFP and beta-galactosidase
809 transformation vectors for promoter/enhancer analysis in Drosophila.
810 *Biotechniques* 29 (4):726, 728, 730, 732.
811 Brand, A.H., and N. Perrimon, 1993 Targeted gene expression as a means of
812 altering cell fates and generating dominant phenotypes. *Development* 118
813 (2):401-415.
814 Calla, B., M. MacLean, L.H. Liao, I. Dhanjal, C. Tittiger *et al.*, 2018 Functional
815 characterization of CYP4G11-a highly conserved enzyme in the western
816 honey bee Apis mellifera. *Insect Mol Biol* 27 (5):661-674.
817 Caputo, B., F.R. Dani, G.L. Horne, V. Petrarca, S. Turillazzi *et al.*, 2005 Identification
818 and composition of cuticular hydrocarbons of the major Afrotropical malaria
819 vector Anopheles gambiae s.s. (Diptera: Culicidae): analysis of sexual
820 dimorphism and age-related changes. *J Mass Spectrom* 40 (12):1595-1604.
821 Carter, M.J., and I.D. Milton, 1993 An inexpensive and simple method for DNA
822 purifications on silica particles. *Nucleic Acids Res* 21 (4):1044.
823 Chen, N., Y.L. Fan, Y. Bai, X.D. Li, Z.F. Zhang *et al.*, 2016 Cytochrome P450 gene,
824 CYP4G51, modulates hydrocarbon production in the pea aphid,
825 Acyrthosiphon pisum. *Insect Biochem Mol Biol* 76:84-94.
826 Chen, X.G., G. Mathur, and A.A. James, 2008 Gene expression studies in
827 mosquitoes. *Adv Genet* 64:19-50.
828 Chiang, Y.N., K.J. Tan, H. Chung, O. Lavrynenko, A. Shevchenko *et al.*, 2016
829 Steroid Hormone Signaling Is Essential for Pheromone Production and
830 Oenocyte Survival. *PLoS Genet* 12 (6):e1006126.
831 Christophers, S.R., 1960 *Aëdes aegypti (L.), the yellow fever mosquito; its life*
832 *history, bionomics, and structure*. Cambridge Eng.: University Press.
833 Combs, P.A., J.J. Krupp, N.M. Khosla, D. Bua, D.A. Petrov *et al.*, 2018 Tissue-
834 Specific cis-Regulatory Divergence Implicates eloF in Inhibiting Interspecies
835 Mating in Drosophila. *Curr Biol* 28 (24):3969-3975 e3963.
836 Gill, G., and M. Ptashne, 1988 Negative effect of the transcriptional activator GAL4.
837 *Nature* 334 (6184):721-724.
838 Gould, A.P., P.R. Elstob, and V. Brodu, 2001 Insect oenocytes: a model system for
839 studying cell-fate specification by Hox genes. *J Anat* 199 (Pt 1-2):25-33.
840 Groth, A.C., E.C. Olivares, B. Thyagarajan, and M.P. Calos, 2000 A phage integrase
841 directs efficient site-specific integration in human cells. *Proc Natl Acad Sci U*
842 *S A* 97 (11):5995-6000.
843 Gutierrez, E., D. Wiggins, B. Fielding, and A.P. Gould, 2007 Specialized hepatocyte-
844 like cells regulate Drosophila lipid metabolism. *Nature* 445 (7125):275-280.
845 Hammond, A., R. Galizi, K. Kyrou, A. Simoni, C. Siniscalchi *et al.*, 2016 A CRISPR-
846 Cas9 gene drive system targeting female reproduction in the malaria
847 mosquito vector Anopheles gambiae. *Nat Biotechnol* 34 (1):78-83.

848 Horn, C., B. Jaunich, and E.A. Wimmer, 2000 Highly sensitive, fluorescent
849 transformation marker for Drosophila transgenesis. *Dev Genes Evol* 210
850 (12):623-629.
851 Horn, C., B.G. Schmid, F.S. Pogoda, and E.A. Wimmer, 2002 Fluorescent
852 transformation markers for insect transgenesis. *Insect Biochem Mol Biol* 32
853 (10):1221-1235.
854 Horn, C., and E.A. Wimmer, 2000 A versatile vector set for animal transgenesis. *Dev*
855 *Genes Evol* 210 (12):630-637.
856 Ingham, V.A., C.M. Jones, P. Pignatelli, V. Balabanidou, J. Vontas *et al.*, 2014
857 Dissecting the organ specificity of insecticide resistance candidate genes in
858 Anopheles gambiae: known and novel candidate genes. *BMC Genomics*
859 15:1018.
860 Jones, C.M., K.A. Haji, B.O. Khatib, J. Bagi, J. Mcha *et al.*, 2013 The dynamics of
861 pyrethroid resistance in Anopheles arabiensis from Zanzibar and an
862 assessment of the underlying genetic basis. *Parasit Vectors* 6:343.
863 Joseph, N.M., N.Y. Elphick, S. Mohammad, and J.H. Bauer, 2018 Altered
864 pheromone biosynthesis is associated with sex-specific changes in life span
865 and behavior in Drosophila melanogaster. *Mech Ageing Dev* 176:1-8.
866 Kefi, M., V. Balabanidou, V. Douris, G. Lycett, R. Feyereisen *et al.*, 2019 Two
867 functionally distinct CYP4G genes of Anopheles gambiae contribute to
868 cuticular hydrocarbon biosynthesis. *Insect Biochem Mol Biol* 110:52-59.

869 Khoury, G., and P. Gruss, 1983 Enhancer elements. *Cell* 33 (2):313-314.

870 Livak, K.J., 1984 Organization and mapping of a sequence on the Drosophila
871 melanogaster X and Y chromosomes that is transcribed during
872 spermatogenesis. *Genetics* 107 (4):611-634.
873 Lombardo, F., G.J. Lycett, A. Lanfrancotti, M. Coluzzi, and B. Arca, 2009 Analysis of
874 apyrase 5' upstream region validates improved Anopheles gambiae
875 transformation technique. *BMC Res Notes* 2:24.
876 Lycett, G.J., D. Amenya, and A. Lynd, 2012 The Anopheles gambiae alpha-tubulin-
877 1b promoter directs neuronal, testes and developing imaginal tissue specific
878 expression and is a sensitive enhancer detector. *Insect Mol Biol* 21 (1):79-88.
879 Lycett, G.J., F.C. Kafatos, and T.G. Loukeris, 2004 Conditional expression in the
880 malaria mosquito Anopheles stephensi with Tet-On and Tet-Off systems.
881 *Genetics* 167 (4):1781-1790.
882 Lycett, G.J., L.A. McLaughlin, H. Ranson, J. Hemingway, F.C. Kafatos *et al.*, 2006
883 Anopheles gambiae P450 reductase is highly expressed in oenocytes and in
884 vivo knockdown increases permethrin susceptibility. *Insect Mol Biol* 15
885 (3):321-327.
886 Lynd, A., and G.J. Lycett, 2011 Optimization of the Gal4-UAS system in an
887 Anopheles gambiae cell line. *Insect Mol Biol* 20 (5):599-608.
888 Lynd, A., and G.J. Lycett, 2012 Development of the bi-partite Gal4-UAS system in
889 the African malaria mosquito, Anopheles gambiae. *PLoS One* 7 (2):e31552.
890 MacLean, M., J. Nadeau, T. Gurnea, C. Tittiger, and G.J. Blomquist, 2018 Mountain
891 pine beetle (Dendroctonus ponderosae) CYP4Gs convert long and short
892 chain alcohols and aldehydes to hydrocarbons. *Insect Biochem Mol Biol*
893 102:11-20.
894 Maibeche-Coisne, M., L. Monti-Dedieu, S. Aragon, and C. Dauphin-Villemant, 2000
895 A new cytochrome P450 from Drosophila melanogaster, CYP4G15,

896 expressed in the nervous system. *Biochem Biophys Res Commun* 273
897 (3):1132-1137.
898 Makki, R., E. Cinnamon, and A.P. Gould, 2014 The development and functions of
899 oenocytes. *Annu Rev Entomol* 59:405-425.
900 Mao, W., M.A. Schuler, and M.R. Berenbaum, 2015 Task-related differential
901 expression of four cytochrome P450 genes in honeybee appendages. *Insect*
902 *Mol Biol* 24 (5):582-588.
903 Nimmo, D.D., L. Alphey, J.M. Meredith, and P. Eggleston, 2006 High efficiency site-
904 specific genetic engineering of the mosquito genome. *Insect Mol Biol* 15
905 (2):129-136.
906 O'Brochta, D.A., R.T. Alford, K.L. Pilitt, C.U. Aluvihare, and R.A. Harrell, 2nd, 2011
907 *piggyBac* transposon remobilization and enhancer detection in Anopheles
908 mosquitoes. *Proc Natl Acad Sci U S A* 108 (39):16339-16344.
909 O'Brochta, D.A., K.L. Pilitt, R.A. Harrell, 2nd, C. Aluvihare, and R.T. Alford, 2012
910 Gal4-based enhancer-trapping in the malaria mosquito Anopheles stephensi.
911 *G3 (Bethesda)* 2 (11):1305-1315.
912 Parvy, J.P., L. Napal, T. Rubin, M. Poidevin, L. Perrin *et al.*, 2012 Drosophila
913 melanogaster Acetyl-CoA-carboxylase sustains a fatty acid-dependent remote
914 signal to waterproof the respiratory system. *PLoS Genet* 8 (8):e1002925.
915 Pitts, R.J., D.C. Rinker, P.L. Jones, A. Rokas, and L.J. Zwiebel, 2011 Transcriptome
916 profiling of chemosensory appendages in the malaria vector Anopheles
917 gambiae reveals tissue- and sex-specific signatures of odor coding. *BMC*
918 *Genomics* 12:271.
919 Pondeville, E., N. Puchot, J.M. Meredith, A. Lynd, K.D. Vernick *et al.*, 2014 Efficient
920 PhiC31 integrase-mediated site-specific germline transformation of Anopheles
921 gambiae. *Nat Protoc* 9 (7):1698-1712.
922 Povelones, M., R.M. Waterhouse, F.C. Kafatos, and G.K. Christophides, 2009
923 Leucine-rich repeat protein complex activates mosquito complement in
924 defense against Plasmodium parasites. *Science* 324 (5924):258-261.
925 Qiu, Y., C. Tittiger, C. Wicker-Thomas, G. Le Goff, S. Young *et al.*, 2012b An insect-
926 specific P450 oxidative decarbonylase for cuticular hydrocarbon biosynthesis.
927 *Proc Natl Acad Sci U S A* 109 (37):14858-14863.
928 Reid, W., K. Pilitt, R. Alford, A. Cervantes-Medina, H. Yu *et al.*, 2018 An Anopheles
929 stephensi Promoter-Trap: Augmenting Genome Annotation and Functional
930 Genomics. *G3 (Bethesda)* 8 (10):3119-3130.
931 Stefana, M.I., P.C. Driscoll, F. Obata, A.R. Pengelly, C.L. Newell *et al.*, 2017
932 Developmental diet regulates Drosophila lifespan via lipid autotoxins. *Nat*
933 *Commun* 8 (1):1384.
934 Xiao, Y.H., M.H. Yin, L. Hou, and Y. Pei, 2006 Direct amplification of intron-
935 containing hairpin RNA construct from genomic DNA. *Biotechniques* 41
936 (5):548, 550, 552.
937 Yu, Z., X. Zhang, Y. Wang, B. Moussian, K.Y. Zhu *et al.*, 2016 LmCYP4G102: An
938 oenocyte-specific cytochrome P450 gene required for cuticular waterproofing
939 in the migratory locust, Locusta migratoria. *Sci Rep* 6:29980.

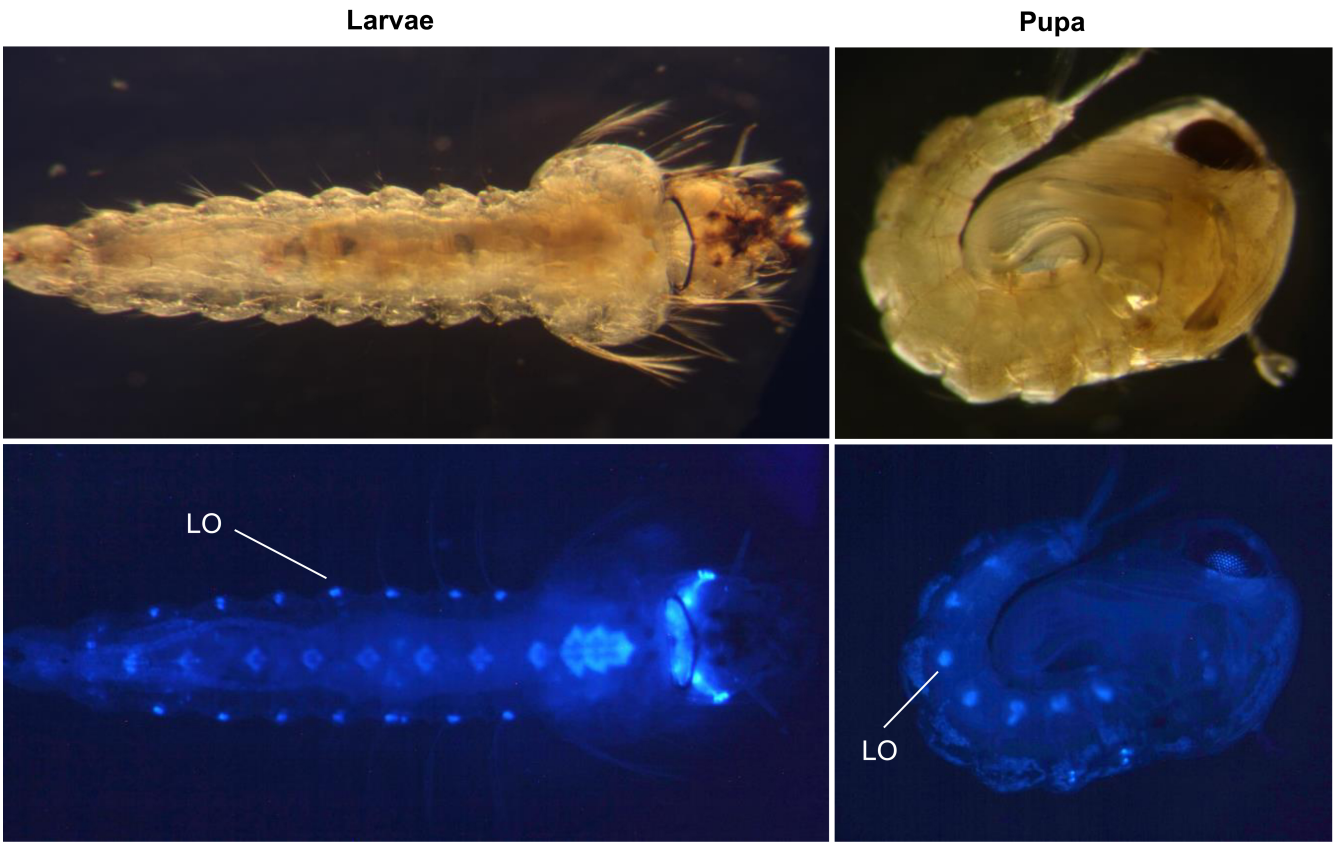
Larvae
Pupa
LO
LO

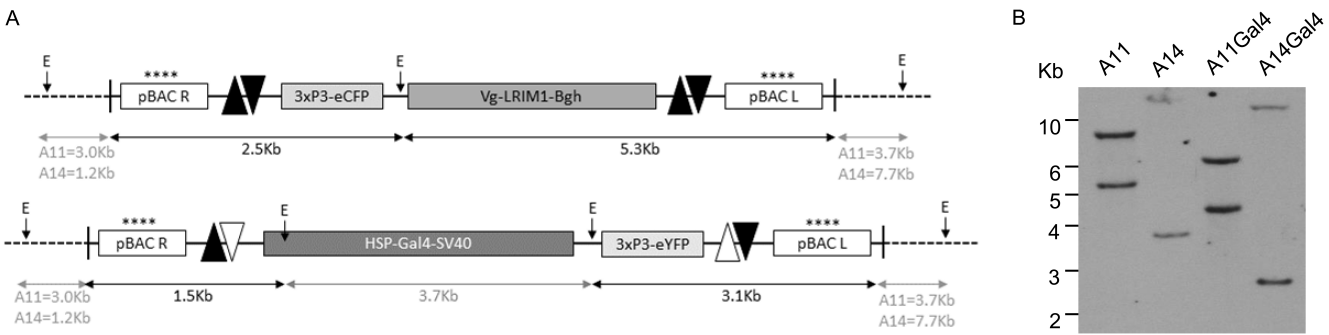
A
E
****
pBAC R
3xP3-eCFP
Vg-LRIM1-Bgh
pBAC L
A11=3.0Kb
A14=1.2Kb
2.5Kb
5.3Kb
A11=3.7Kb
A14=7.7Kb
HSP-Gal4-SV40
3xP3-eYFP
1.5Kb
3.7Kb
3.1Kb
B
Kb
A11
A14
A11Gal4
A14Gal4
10
6
5
4
3
2

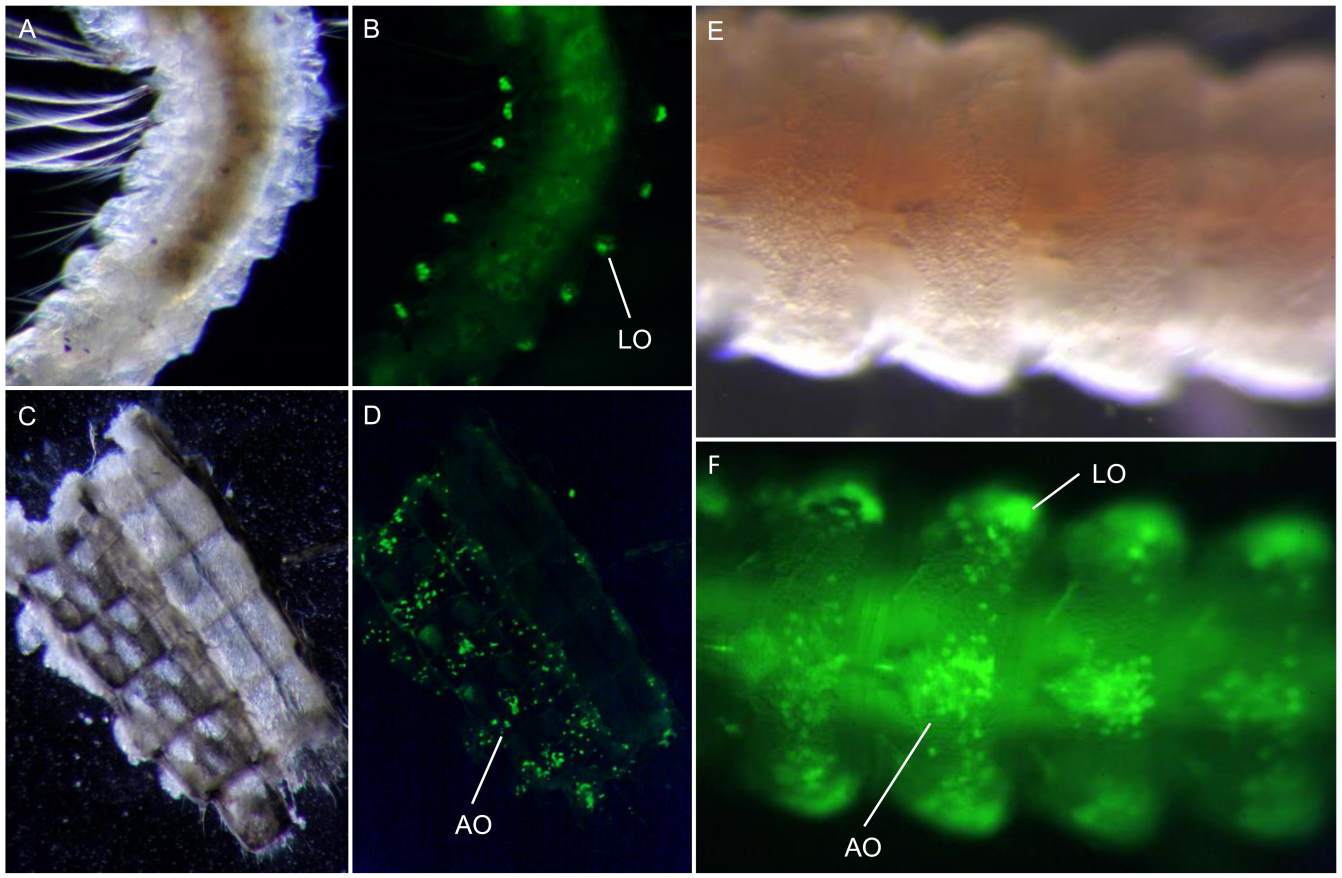
A
B
LO
E
C
D
AO
F
LO
AO

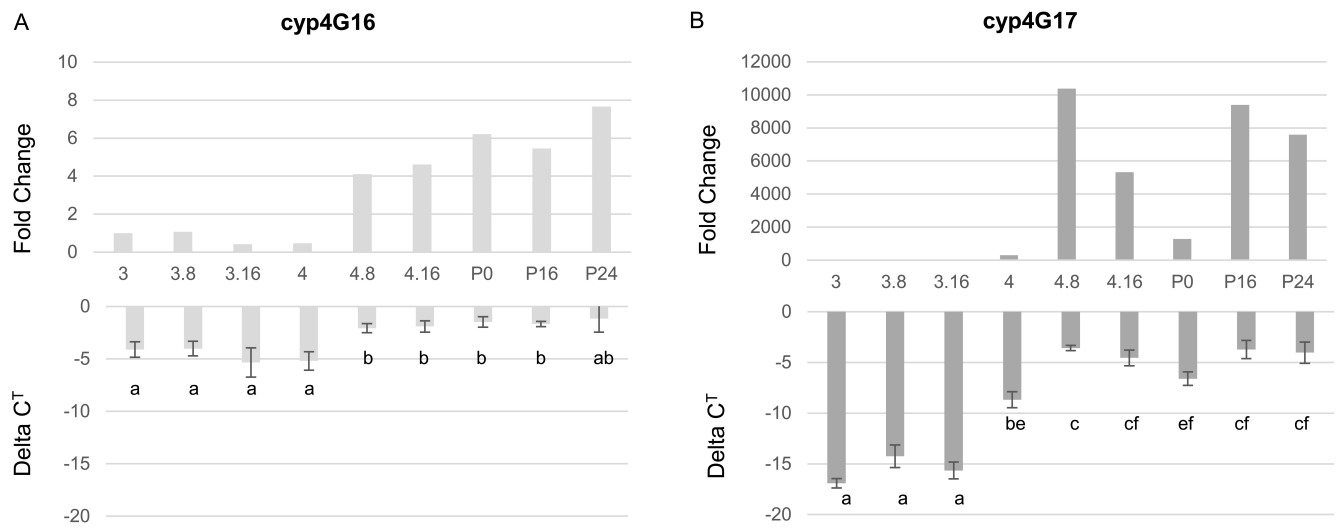
A
cyp4G16
Fold Change
10
8
6
4
2
0
3
3.8
3.16
4
4.8
4.16
P0
P16
P24
Delta C^T
0
-5
-10
-15
-20
a
a
a
a
b
b
b
b
ab
B
cyp4G17
Fold Change
12000
10000
8000
6000
4000
2000
0
3
3.8
3.16
4
4.8
4.16
P0
P16
P24
Delta C^T
0
-5
-10
-15
-20
a
a
a
be
c
cf
ef
cf
cf

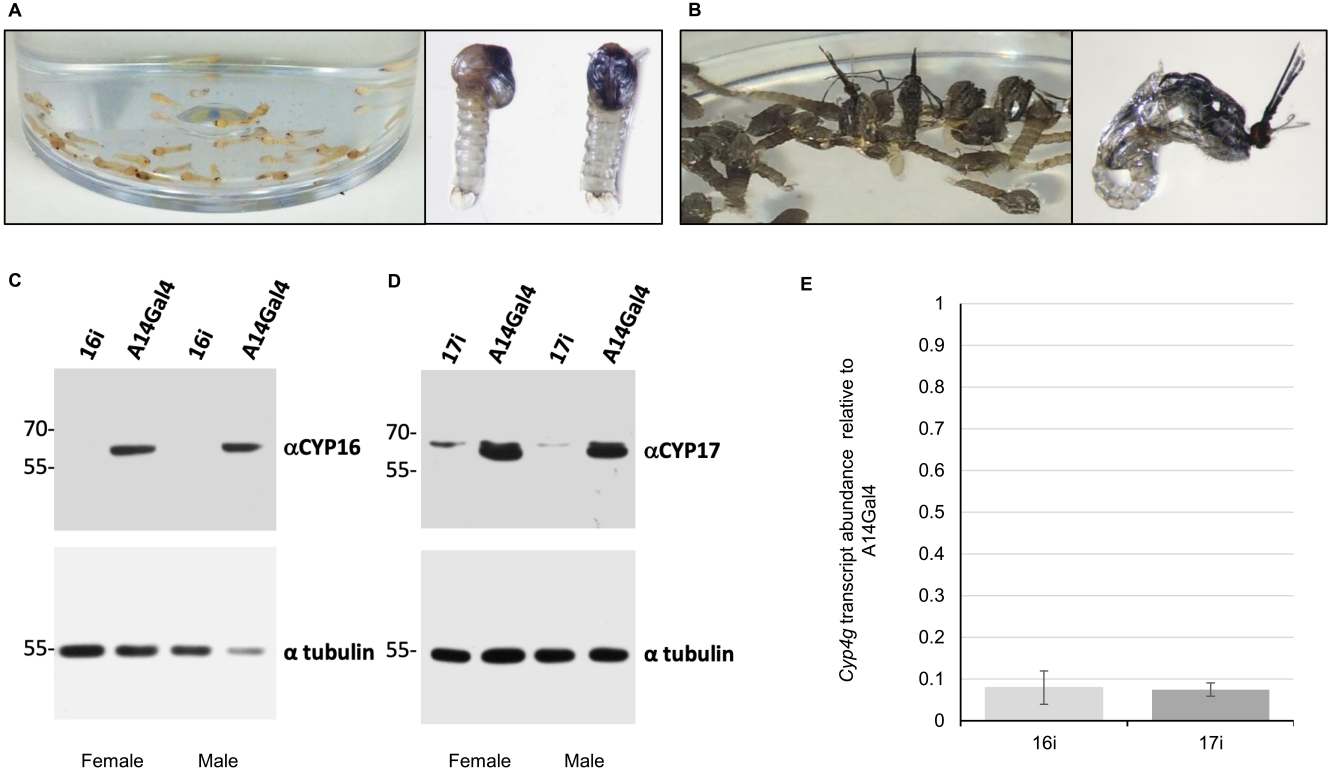
A
B
C
16i
A14Gal4
16i
A14Gal4
70-
55-
αCYP16
55-
α tubulin
Female
Male
D
17i
A14Gal4
17i
A14Gal4
70-
55-
αCYP17
55-
α tubulin
Female
Male
E
Cyp4g transcript abundance relative to A14Gal4
1
0.9
0.8
0.7
0.6
0.5
0.4
0.3
0.2
0.1
0
16i
17i

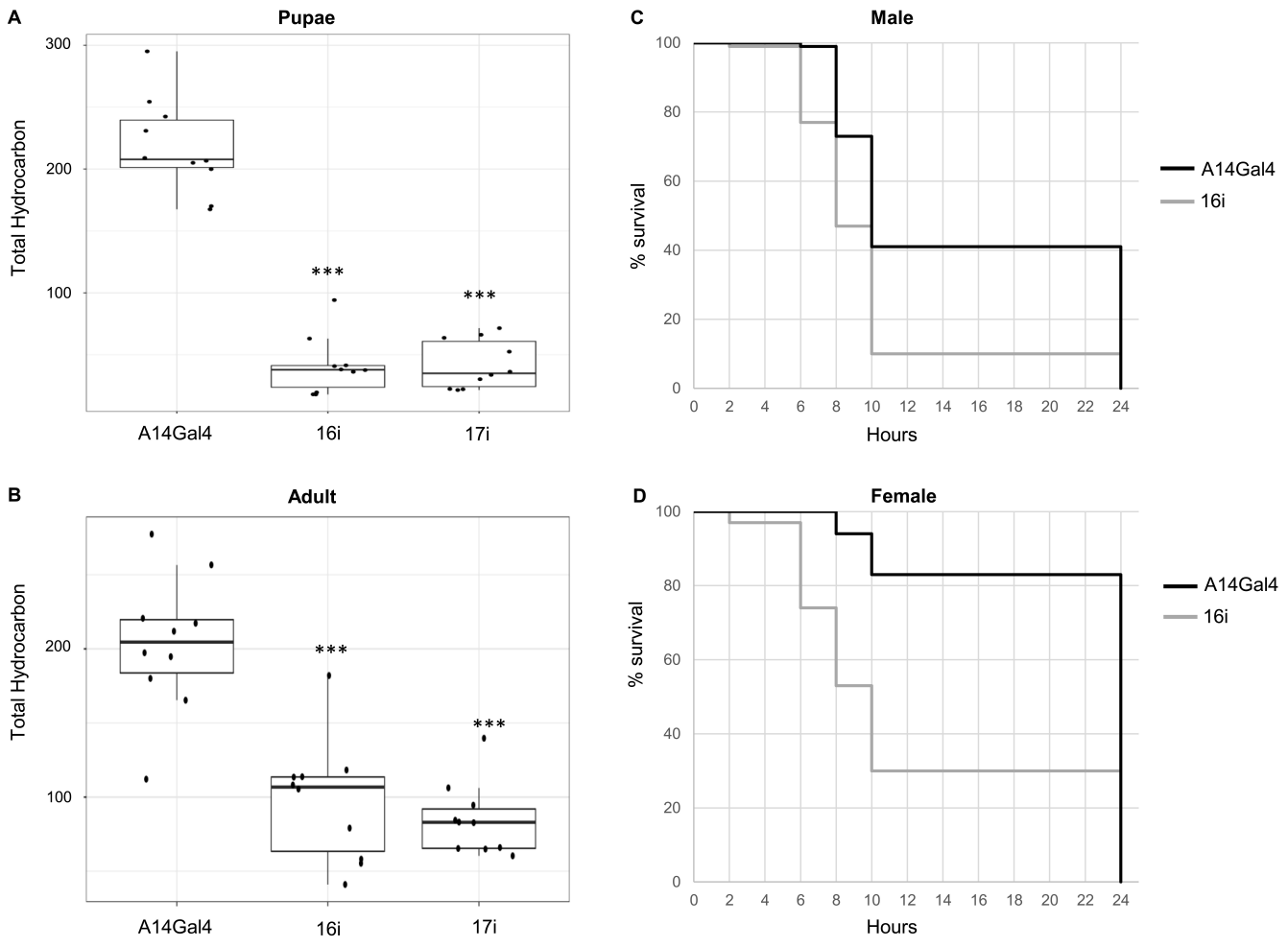
A
Pupae
Total Hydrocarbon
300
200
100
***
***
A14Gal4
16i
17i
B
Adult
Total Hydrocarbon
200
100
***
***
A14Gal4
16i
17i
C
Male
% survival
100
80
60
40
20
0
0 2 4 6 8 10 12 14 16 18 20 22 24
Hours
A14Gal4
16i
D
Female
% survival
100
80
60
40
20
0
0 2 4 6 8 10 12 14 16 18 20 22 24
Hours
A14Gal4
16i